Peculiarly strong room-temperature ferromagnetism from low Mn-doping in ZnO grown by molecular beam epitaxy

Zheng Zuo, Muhammad Morshed, W. P. Beyermann, Jian-Guo Zheng, Yan Xin et al.

Related Articles

Investigation of the origin of glassiness in La0.5Sr0.5CoO3
J. Appl. Phys. 113, 17E114 (2013)

Stabilization of the in-plane vortex state in two-dimensional circular nanorings
J. Appl. Phys. 113, 093901 (2013)

Effect of longitudinal degree of freedom of magnetic moment in body-centered-cubic iron
J. Appl. Phys. 113, 17E112 (2013)

Magnetic structure of GdNiSn
J. Appl. Phys. 113, 17E107 (2013)

Role of covalent hybridization in the martensitic structure and magnetic properties of shape-memory alloys: The case of Ni50Mn5+xGa35-xCu10
Appl. Phys. Lett. 102, 062407 (2013)

Additional information on AIP Advances

Journal Homepage: http://aipadvances.aip.org

Journal Information: http://aipadvances.aip.org/about/journal

Top downloads: http://aipadvances.aip.org/most_downloaded

Information for Authors: http://aipadvances.aip.org/authors

Peculiarly strong room-temperature ferromagnetism from low Mn-doping in ZnO grown by molecular beam epitaxy

Zheng Zuo,[1] Muhammad Morshed,[1] W. P. Beyermann,[2] Jian-Guo Zheng,[3] Yan Xin,[4] and Jianlin Liu[1,a]

[1]*Quantum Structures Laboratory, Department of Electrical Engineering, University of California at Riverside, Riverside, California 92521, USA*
[2]*Department of Physics and Astronomy, University of California at Riverside, Riverside, California 92521, USA*
[3]*Laboratory for Electron and X-ray Instrumentation, California Institute for Telecommunications and Information Technology, University of California Irvine, Irvine, California 92697, USA*
[4]*NHMFL, Florida State University, 1800 E. Paul Dirac Dr., Tallahassee, FL 32310-3706, USA*

Strong room-temperature ferromagnetism is demonstrated in single crystalline Mn-doped ZnO thin films grown by molecular beam epitaxy. Very low Mn doping concentration is investigated, and the measured magnetic moment is much larger than what is expected for an isolated ion based on Hund's rules. The ferromagnetic behavior evolves with Mn concentration. Both magnetic anisotropy and anomalous Hall effect confirm the intrinsic nature of ferromagnetism. While the Mn dopant plays a crucial role, another entity in the system is needed to explain the observed large magnetic moments. *Copyright 2013 Author(s). This article is distributed under a Creative Commons Attribution 3.0 Unported License.* [http://dx.doi.org/10.1063/1.4794799]

I. INTRODUCTION

Diluted magnetic semiconductors (DMS) have attracted much attention for their potential in spintronic applications.[1–3] Early investigations in MnGaAs had been quite successful with the only obstacle being their low Curie temperature.[4] Transition metal (TM) doped ZnO materials are expected to have Curie temperatures above 300K,[1,5] which led to a surge in research activities. Extensive work has been performed on synthesizing TM doped ZnO using various methods, including chemical reaction,[6,7] sintering,[8,9] ion implantation,[10–12] sputtering,[13] pulsed laser deposition,[14] metal-organic chemical vapor deposition[15] and molecular beam epitaxy (MBE).[16–18] Among these methods, MBE provides high quality thin films and precise doping profiles. Mn-doped ZnO is of particular interest since it lacks room-temperature ferromagnetic Mn-rich phases.[19] Original predictions based on the p-d Zender model required very high p-type doping for MnZnO to be a room temperature DMS,[5] which is very challenging to fulfill. Nevertheless many different types of behavior have been reported with MnZnO, such as being non-magnetic,[7] paramagnetic,[13] ferromagnetic,[8,17,18] antiferromagnetic,[20] and spin-glass like,[14] with no evident instance of the required heavy p-type doping. Other theories based on bound magnetic polarons (BMP),[21,22] F centers,[23] etc. forgo such requirements on carrier type and concentration, although other factors are introduced. One area that remains to be fully explored is low concentration Mn doping (below 0.1 at.%). An early report on MnZnO with a Mn concentration of $\sim$0.2 at.% showed magnetic moments larger than $1\mu_B$/ion.[24] Recently, we also observed strong ferromagnetism at room temperature in MnZnO with a low Mn concentration of 2×10^{19} cm^{-3}.[18] In this paper we report MBE growth of a series of high-quality single crystalline Mn-doped ZnO thin films with very low Mn concentration and their magnetic

---

[a]Corresponding author. Tel.: +1-951-8277131, Fax: +1-951-8272425, E-mail address: jianlin@ee.ucr.edu

properties. Again peculiarly strong RT ferromagnetism is observed with a per ion magnetic moment larger than isolated ion based on Hund's rules. The strength of the ferromagnetism is found to evolve with the Mn concentration.

II. EXPERIMENTS

Mn-doped ZnO thin films were grown using electron cyclotron resonance (ECR)-MBE. Radical Knudsen effusion cells filled with elemental Zn (6N) and Mn (5.5N) metals were used as Zn and Mn sources. The Zn and Mn fluxes were controlled by the effusion cell temperatures. An ECR plasma tube supplied with O_2 (5N) gas was used as the oxygen source, and the oxygen flow rate was precisely tuned by a mass flow controller. The films were grown on r-sapphire substrates (Rubicon). The substrates were cleaned in boiling aqua regia solution for 50 minutes before DI water rinsing and blown dry by nitrogen. Samples were then annealed in vacuum at 800°C for 30 minutes. A low temperature ZnO buffer was grown at 450°C. The buffer growth lasted 5 minutes with an estimated thickness of 1–2 nm. During the growth, the Zn cell temperature and O_2 flow rate were kept at 430°C and 14 sccm, respectively. For Mn doped samples the Mn cell temperature was set at 500°C – 800°C. The substrate temperature was 650°C, and the growths lasted 2 hours. An annealing at 800°C for 30 minutes was performed after growth in vacuum. A reference sample was grown with the same growth procedure without Mn flux. The thickness of the films was measured using a Dektak 8 Surface Profilometer. X-ray diffraction (XRD) measurements were performed using a Bruker D8 Advance X-ray diffractometer. Photoluminescence (PL) study was carried out using a home-built PL system with a Janis cryostat, a 325 nm He-Cd laser for the excitation source and a photomultiplier tube for the PL detection. Cross-sectional transmission electron microscopy (TEM) specimens were prepared in a FEI Quanta 3D FEG dual-beam focused ion beam (FIB) system, and diffraction contrast TEM imaging and selected area electron diffraction (SAED) were carried out in a FEI/Philips CM-20 TEM at the materials characterization facility (LEXI) in UC Irvine. High-resolution TEM was performed in a JEOL JEM ARM200F TEM at the Florida State University. The magnetic properties of the samples were characterized using a Quantum Design MPMS SQUID magnetometer. Magneto-transport properties were investigated using a Quantum Design PPMS system.

III. RESULTS AND DISCUSSION

Figure 1(a) and 1(b)–1(h) show reflection high energy electron diffraction (RHEED) patterns of both undoped ZnO and Mn doped ZnO films, respectively. The patterns were acquired within the MBE chamber after growth at room temperature. The streaky patterns indicate smooth surface on all samples, as befitting high quality growth by MBE, and there is no evident difference among the series of samples.

Figure 2(a) and 2(b)–2(h) show XRD patterns of both undoped ZnO and Mn doped ZnO, respectively. The θ-2θ scan shows peaks for r-sapphire ($1\bar{1}02$) as well as A-plane ($11\bar{2}0$) ZnO. The pattern indicates that the film is single crystal and the ($11\bar{2}0$) plane of the film is parallel to the ($1\bar{1}02$) plane of the substrate, which fits the epitaxial relationship of ZnO grown on r-sapphire.[19] None of the other ZnO directions are observed due to the high-quality epitaxial growth by MBE. No Mn-rich secondary phases are detected either. Finally, no peak shift is observed among the samples indicating the doping levels are so low that they neither affect the lattice parameter, nor result in alloying.

Figure 3(a) shows a bright-field cross-sectional TEM image of Mn doped ZnO grown on sapphire at the Mn cell temperature of 800°C. The film contains dislocations which cause contrast variations in the image. However, no Mn-rich secondary phases were observed. X-ray Energy Dispersive Spectroscopy (EDS) measurements were performed on the sample and no Mn signals show up in EDS spectra, suggesting that the Mn concentration is below EDS detection limit. The SAED pattern in Figure 3(b) clearly shows two sets of diffraction patterns, which are related to the sapphire substrate and Mn doped ZnO thin film, respectively. These patterns reveal the single-crystalline nature of the thin film and epitaxial growth. They also confirm that the film ($11\bar{2}0$) plane is parallel to the substrate
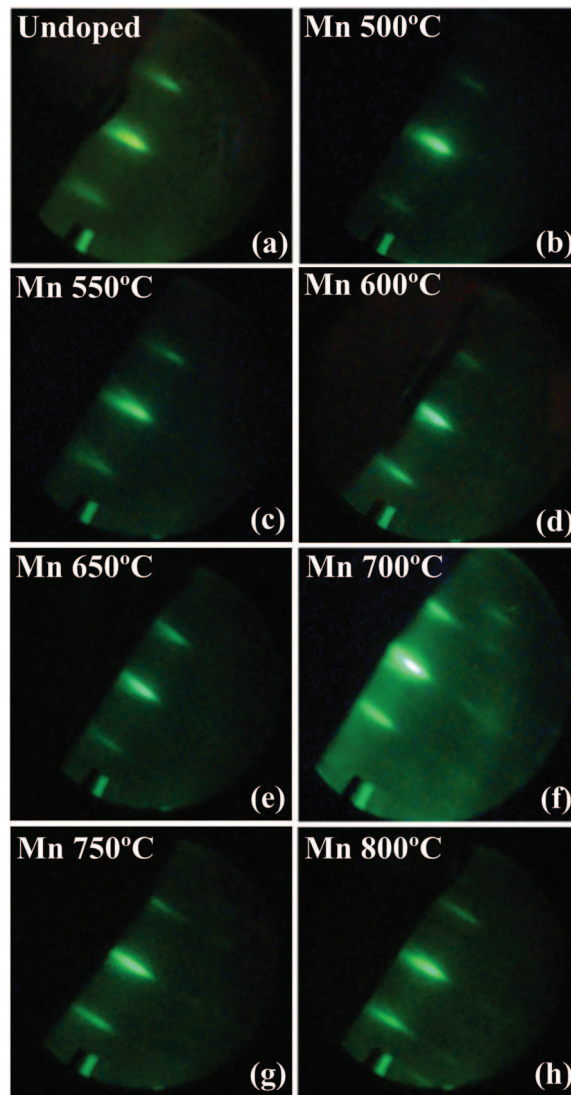
FIG. 1. RHEED patterns of (a) undoped ZnO and (b) ∼ (h) Mn doped ZnO after growth taken at room temperature for Mn cell temperature of 500°C ∼ 800°C. The streaky patterns of all samples indicate smooth surface for all of them.

($1\bar{1}02$) plane, which is consistent with the XRD results. Figure 3(c) is a high resolution TEM image of the same sample, showing high quality single crystalline growth. Fast Fourier Transform (FFT) patterns of three selected areas are also shown in Figure 3(c), indicating clear distinction between Mn doped ZnO and sapphire substrate. The patterns, together with SAED pattern, and TEM images prove that single crystalline ZnO was grown.

Mn doping was controlled by varying Mn cell temperature from 500 °C to 800 °C. Various methods were attempted to assess Mn concentrations. XPS spectra were collected on all samples. Figure 4(a) and 4(b) show XPS spectra of undoped ZnO and Mn doped ZnO with a Mn cell temperature of 800°C, respectively. There is no evident difference between the two spectra at the Mn(2p) binding energy of ∼640 eV, i.e. no evident Mn signal can be observed even from the most heavily doped sample. Figure 4(c) summarizes the Zn to O signal ratio in the XPS spectra of all samples with undoped sample marked as a Mn cell temperature of zero. The Zn to O signal ratio is similar for all samples, indicating no evident deviation from undoped ZnO growth. Figure 5 shows SIMS spectra of Mn doped ZnO with various Mn cell temperatures. As indicated by the signal of Al from sapphire substrate, all thin films have similar thickness of ∼25nm, which is close
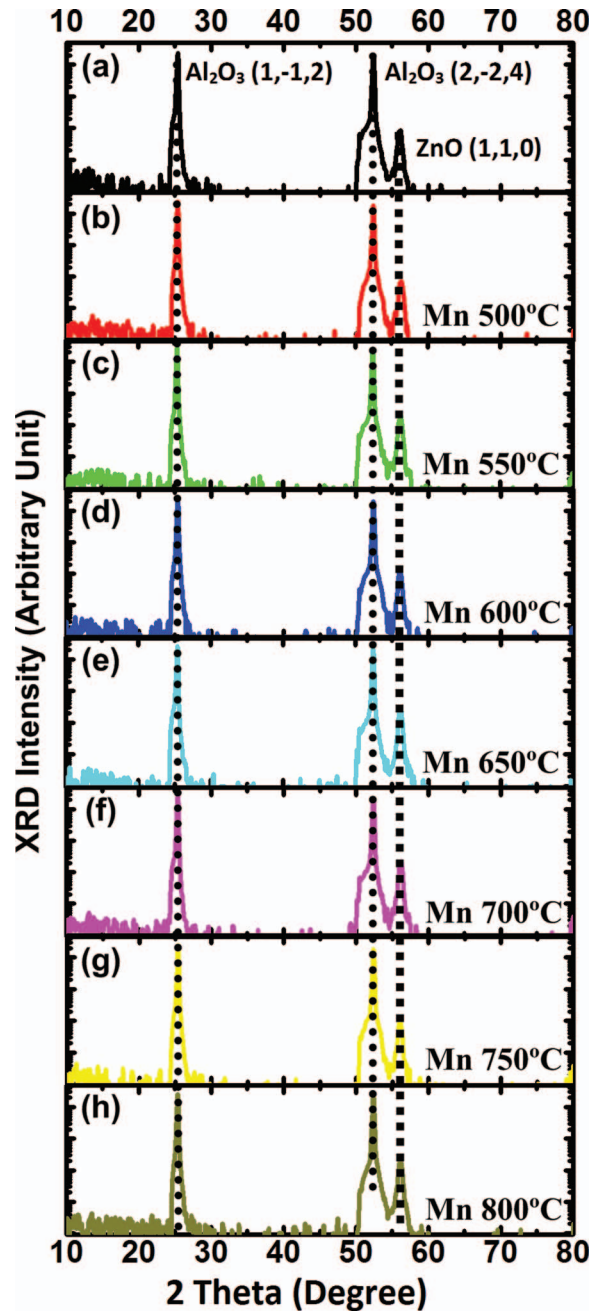
FIG. 2. XRD patterns of (a) undoped ZnO and (b) ~ (h) Mn doped ZnO at different Mn cell temperature. Only ZnO and sapphire related peaks are present and there is no evident secondary phase within detection limit. No evident peak shift is observed.

to the results measured by the profilometer. All figures were aligned by aligning Zn signal to an atomic concentration $\sim 4 \times 10^{22}$ cm^{-3}. When Mn cell temperature is low at 500°C and 600°C, as in Figure 5(a) and 5(b), the Mn signals are on the order of 10^{18} cm^{-3} and are actually close to system noise, meaning an extremely low concentration. Figure 5(c) shows SIMS spectra of the sample with Mn cell temperature 700°C in which a $\sim 1 \times 10^{19}$ cm^{-3} Mn concentration is acquired. This leads to a number of ~ 0.02 at.% Mn content. Figure 5(d) shows SIMS spectra of the sample with Mn cell temperature 800°C. The Mn signal has a slope in this sample, but it is reasonable to assess that the Mn concentration in this sample is less than 1×10^{20} cm^{-3}, or 0.2 at.%. So all doping
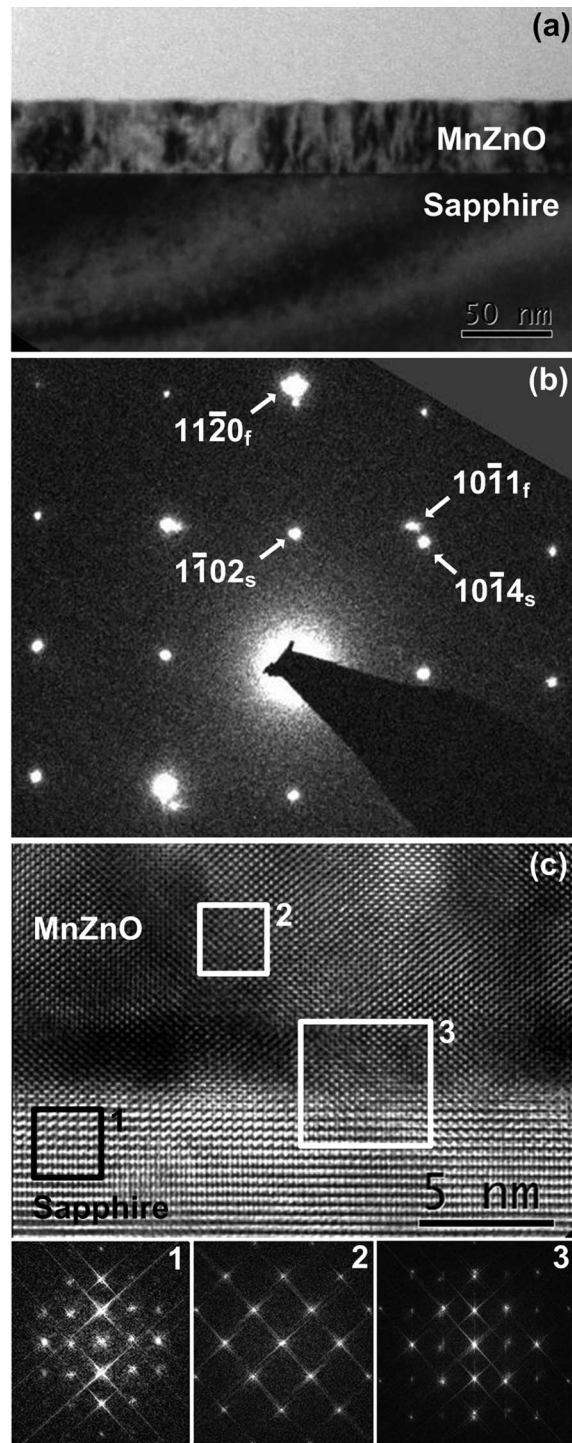
FIG. 3. (a) Cross-sectional TEM image of Mn doped ZnO sample with Mn cell temperature of 800ºC, (b) Two sets of SAED patterns, belonging to the sapphire substrates and single-crystalline Mn doped ZnO thin film, respectively. (c) High resolution TEM image and selected-area FFT patterns, showing single crystalline Mn doped ZnO on sapphire.
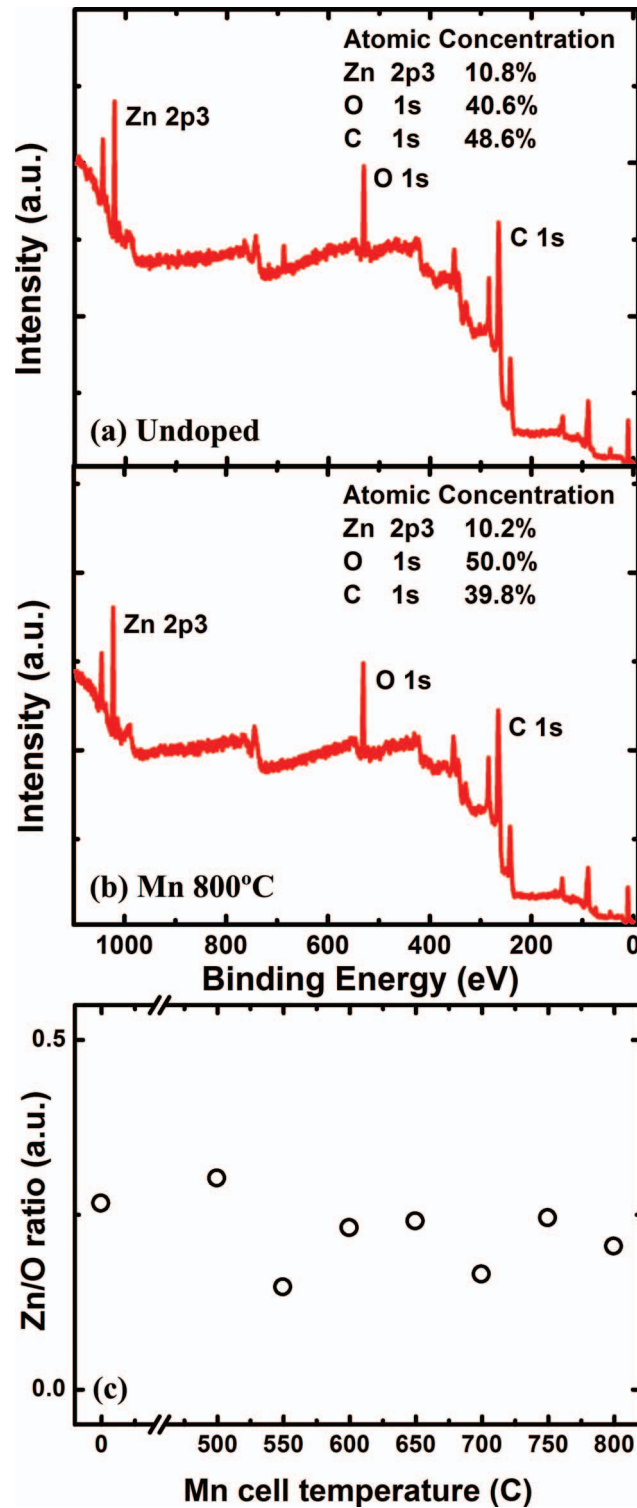
FIG. 4. XPS spectra of (a) undoped ZnO and (b) Mn doped ZnO with Mn cell temperature of 800°C. (c) Zn/O signal ratio from XPS spectra of all samples, indicating minor variance. No spectra have any evident Mn signal, indicating low concentration.
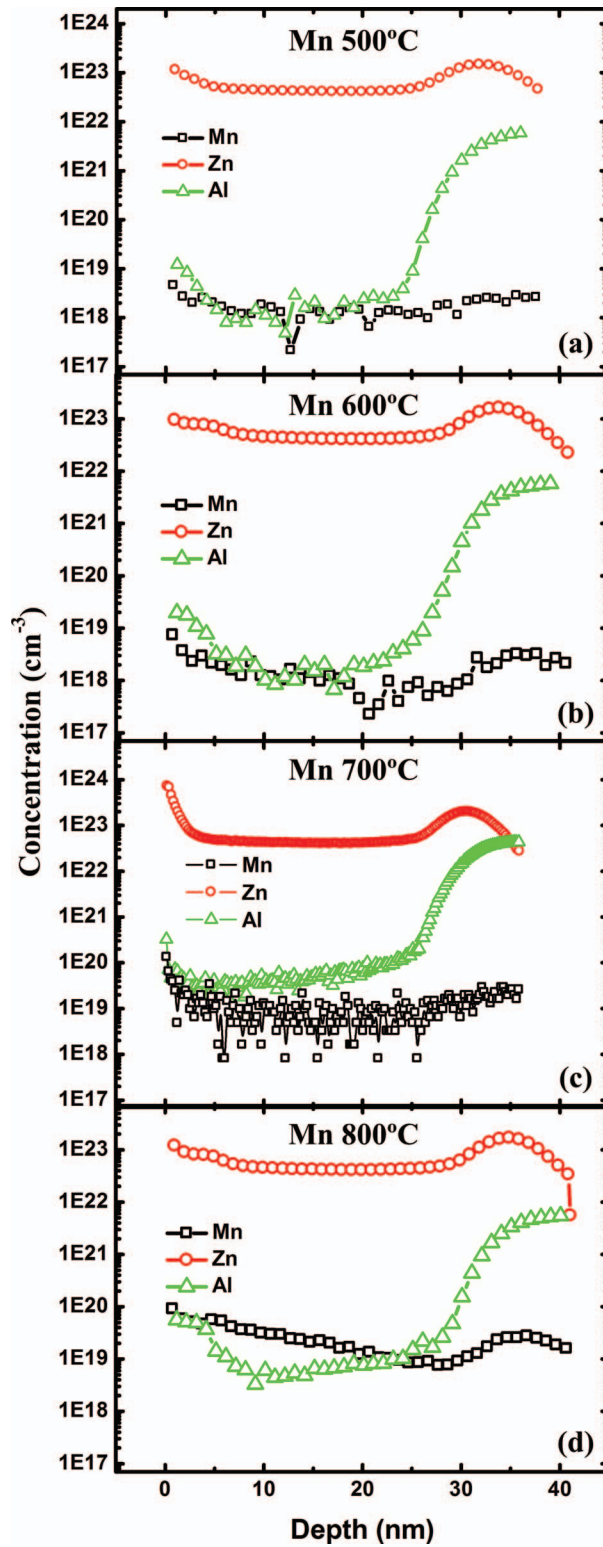
FIG. 5. SIMS spectra of Mn doped ZnO with Mn cell temperature at (a) 500°C, (b) 600°C, (c) 700°C, and (d) 800°C. All concentrations were aligned by Zn signal. Mn signals in (a) and (b) are very low and approach noise level. Signals in (c) and (d) are higher, but still within 0.1%at. This indicates that the Mn doping amount is very low and alloying is excluded.

concentrations in this series of samples are way below the reported incorporation limit,[25] and thus exclude the chance of Mn phase segregation.

Magnetic measurements were performed by mounting cleaved ZnO/Mn-doped ZnO samples in non-magnetic straws. Precautions were taken to prevent extrinsic signals.[26] Carbon-tipped tweezers were used during preparation to avoid iron based tool contamination. Samples were held in position by extra straws placed inside the mounting straw, thus excluding contamination signals from tapes or pastes. Figure 6(a) shows the magnetic moment as a function of external field for undoped ZnO, and the behavior is diamagnetic, associated with both the thin film and substrate. This result suggests that the undoped ZnO does not exhibit ferromagnetism. At a Mn cell temperature of 500°C, a small change is seen in the magnetic response in Figure 6(b), but the signal is still clearly diamagnetic. When the Mn cell temperature is increased beyond 500°C, there is sudden onset of hysteretic behavior, clearly indicating the presence of ferromagnetism. Notice that for Figures 6(c) through 6(h), the linear diamagnetic signal was subtracted from the raw data. As can be seen, room temperature ferromagnetism is evident for samples with a Mn cell temperature of 550°C and higher. Ferromagnetic hysteresis remains similar at different measurement temperature, and the temperature dependence of the saturation moment is not significant for each sample. The magnetic behavior is summarized in Figure 7. Figure 7(a) is the saturation moments (M_s) and residue moments (M_r) for the six samples with evident ferromagnetism. The saturation moment reaches a maximum when the Mn cell temperature is 600°C. Further increases of the Mn cell temperature lead to lower saturation moments with a minimum at 750 °C, followed by a small increase at 800 °C. Figure 7(b) shows the coercivity field of Mn doped ZnO samples. At room temperature, the coercivity starts out at ∼50 Oe for a Mn cell temperature of 500 °C and gradually increases to 100 Oe when cell temperature is 800 °C. The exception to this monotonic trend occurs at 750 °C where it has the exceptionally large value of ∼200 Oe. In most samples the coercivity field increases as the measurement temperature decreases, as can be seen by comparing the 10 K and 300 K data. The one exception is with the Mn cell temperature of 550°C the coercivity does not change with temperature. Figure 7(c) shows the ratio of M_r and M_s, showing a general increasing trend with the increasing Mn cell temperature. The Mn 750°C sample is the anomaly with its larger M_r/M_s ratio and much larger coercivity. Similar behavior was observed in another sample with similar growth parameters,[18] thus we believe this behavior is intrinsic with mechanism that will be discussed later.

Magnetic anisotropy is an important characteristic of intrinsic ferromagnetism. The c-axis of ZnO epitaxially grown on r-sapphire does not align with the growth direction,[19] thus in-plane anisotropy is expected since the thin films are single crystals. For field in-plane measurements, samples were cut into 6mm × 8mm pieces and mounted in a non-magnetic straw, as illustrated in Figure 8(a). We have noticed an easy cleaving direction of r-sapphire, which is closely parallel to its main flat. The factory specification states that the main flat of the substrate is 45° off M on C-plane. Our samples prepared for the magnetic measurements were normally cut with their long edge aligned with the easy cleaving direction, hereon noted as 'cut A'. When they are cut with the short edge aligned with the easy cleaving direction, hereon noted as 'cut B', we observed a larger saturation moment and smaller coercivity field, as can be seen in Figure 8(b). Figure 8(c) shows fielded cooling measurement data for the different cuts in Figure 8(b). An alignment field of 6000 Oe was applied before the measurements were started at 2000 Oe. In both cases, the magnetic moments remain very stable without any abrupt phase change steps during the cooling process. The smooth temperature scan data further proves that no evident secondary phases are present. Figure 9(a) illustrates how out-of-plane anisotropy was measured. The Mn doped ZnO sample was cleaved into a 4mm by 12mm stripe and then cleaved again into three 4mm by 4mm squares, thus providing the same amount of sample as was used for our in-plane measurements. The squares were then stacked together and placed vertically into a nonmagnetic straw for the measurement. As shown in Figure 9(b), the off-plane measurement yields a larger saturation moment than the normal cut A, with a ratio similar to that of in-plane anisotropy. However, the coercivity field remains similar to in-plane reference in this case.

Figure 10 shows the temperature-dependent PL spectra of undoped and Mn-doped ZnO. For undoped ZnO the data in Figure 10(a) shows two well resolved peaks with a donor bound exciton (DX) at 3.362eV and a AES peak at 3.308eV.[27] The broad luminescence bump at ∼3.23eV should
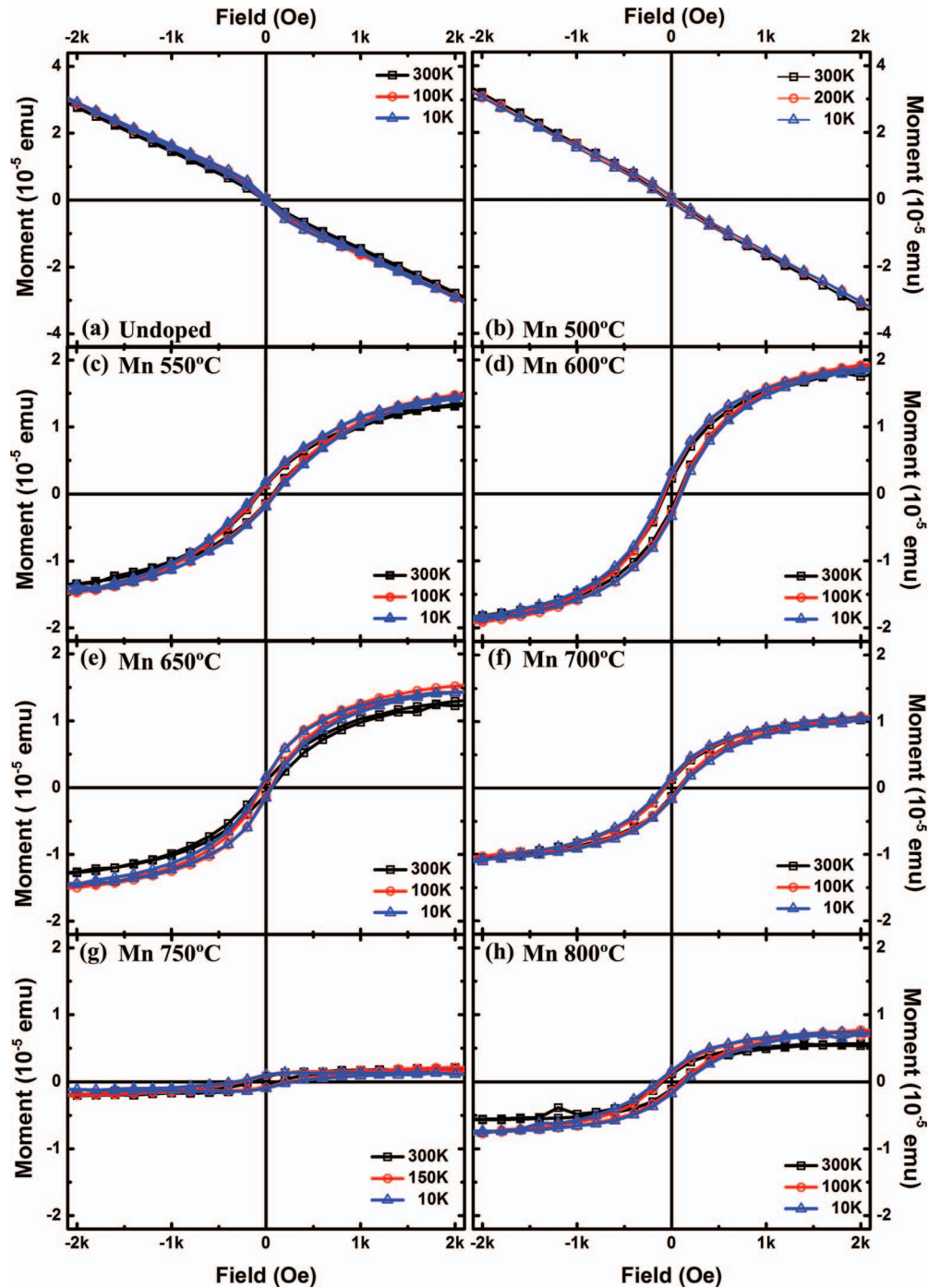
FIG. 6. M-H response of (a) undoped ZnO and (b) ∼ (h) Mn doped ZnO with Mn cell temperature of 500ºC ∼ 800ºC. The undoped ZnO as well as Mn cell temperature 500ºC sample show diamagnetic behavior, while ferromagnetic hysteresis loops are observed on other samples with higher Mn cell temperature. Note that linear term has been removed for the hysteresis graphs in (c) ∼ (h).

consist of multiple peaks like phonon replicas, donor acceptor pairs, etc, which are not resolved enough to be identified. There is a third peak at ∼3.384eV, which is evident at 60K and presents a seemly blue-shift. From a previous polarized PL study,[18] this peak was identified as a DX from a C-band exciton of ZnO. Due to the A-plane ZnO growth, PL from C-band is expected,[28,29] which is evidence of single-crystalline growth. For the Mn doped samples the low-temperature PL behavior is
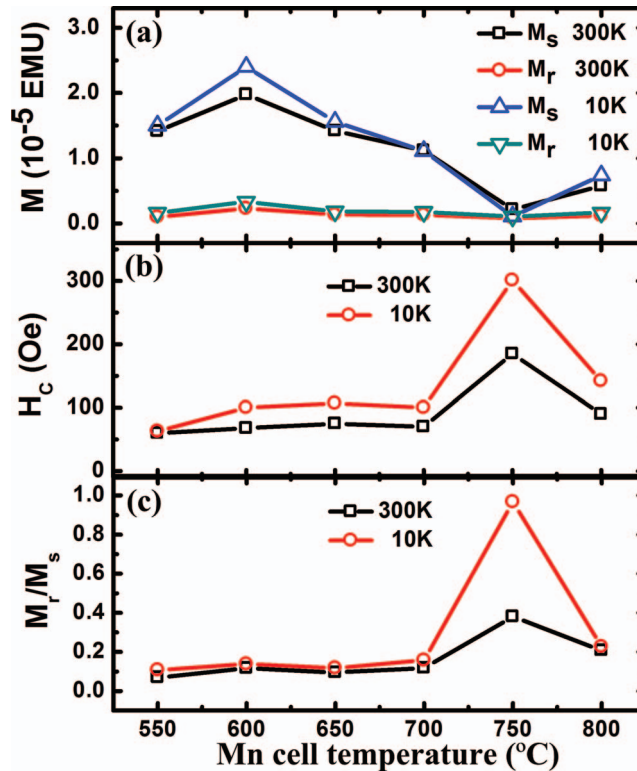
FIG. 7. Summary of the M-H behaviors of the samples. (a) Saturation magnetization (Ms) as well as reminiscent moment at zero fields (Mr) of all samples at 300K and 10K. Ms evolves with rising Mn cell temperature while the change to Mr is less evident. (b) Coercivity field (Hc) and (c) Mr/Ms ratio of the samples. For most samples both Hc and Mr/Ms ratio follow an increasing trend with increased Mn cell temperature. The Mn 750°C sample shows a sudden increase of both Hc and Mr/Ms ratio, which does not follow the trend.

similar in nature but with a slight variance among samples. In the 500°C, 600°C and 800°C samples the dominant high energy peak remains the ∼3.36eV A/B band DX, and a trace of the 3.38eV C-band DX is visible at a slightly elevated measurement temperature, thus providing the blue shift. The AES peak is no longer easily resolvable, but a trace of it can be identified in the Mn 500°C sample. The Mn 700°C sample shows stronger C-band luminescence at low temperature and thus its 'blue-shift' is not evident. The broad luminescence in the Mn 700°C sample is also shifted to higher energy at ∼3.3eV, which is probably due to an enhanced phonon replica from the C-band DX. The exact mechanism of how the C-band signal is enhanced in the Mn 700°C sample remains to be investigated. However it is evident that no additional energy levels were introduced by incorporating Mn at these low doping concentrations.

Figure 11 shows the magneto resistance (MR) of both the undoped and Mn doped samples. For the undoped ZnO as shown in Figure 11(a), a generally negative MR is present at low temperature, as reported for undoped ZnO,[30,31] although there is possibly a weak positive contribution at 200K. For the Mn doped ZnO samples, while the dominant MR response is negative, a stronger positive contribution is evident, and in the anomalous case of Mn 700°C sample, the MR is dominated by a positive contribution at 200K. Figure 12(a) shows the Hall effect data of these samples. While anomalous Hall effect is evident on all of these samples, Mn 800°C sample shows an exceptionally large anomalous term. Figure 12(b) shows the carrier concentrations as extracted from room temperature Hall effect measurements. All samples have very similar electron concentrations of 10^{18} to 10^{19} cm^{-3}, indicating no evident effect on the carrier concentration.

Magnetic anisotropy for both in-plane and out-of-plane cases and anomalous Hall effect suggest that the observed ferromagnetism is intrinsic. However the strength of the magnetic moment becomes peculiar when quantized to per-Mn-ion moment. We had previously reported our findings of a
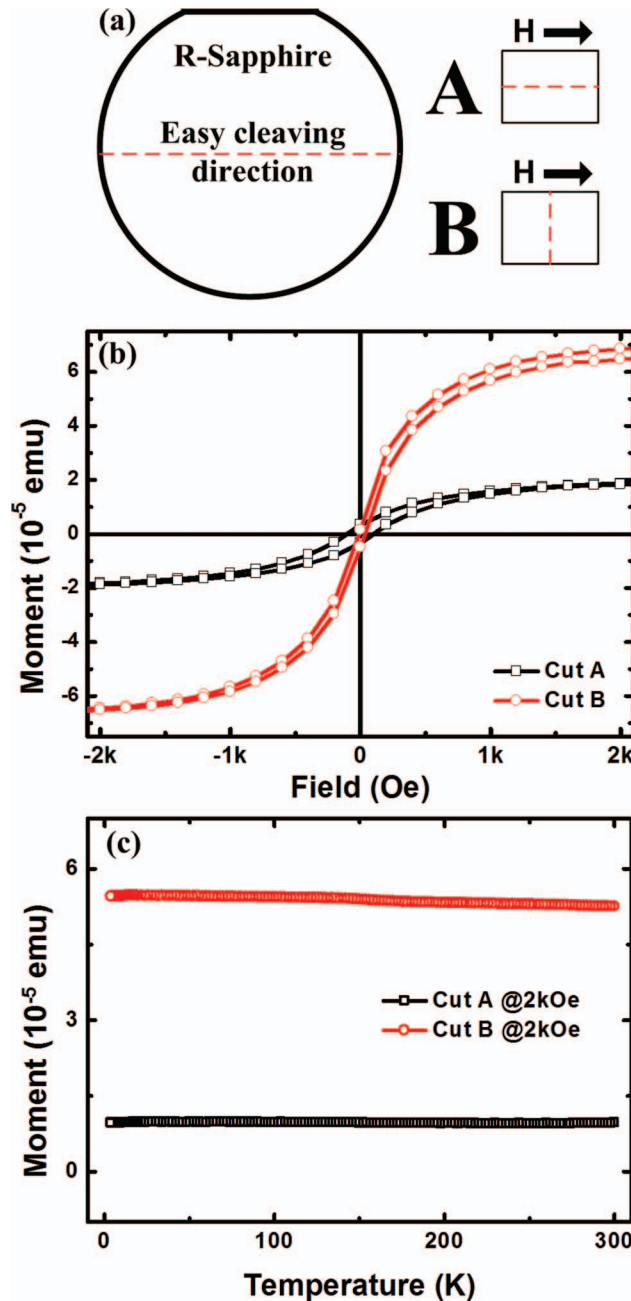
FIG. 8. In-plane magnetic anisotropy of Mn-doped ZnO sample. (a) Schematic of samples aligned by the observed easy-cleaving direction of sapphire substrate. Two cuts of samples with the same shape but crystal direction ~90° apart were used. (b) M-H hysteresis and (c) fielded-cooling result of Mn cell 600°C sample. Cut B shows increased saturation moment and reduced coercivity field. In both cases temperature cooling shows no abrupt phase change steps, supporting intrinsic DMS.

Mn doped ZnO with a similarly low Mn concentration of $\sim 2 \times 10^{19}$ cm^{-3}.[18] That sample was characterized to have $\sim 6\,\mu_B$/ion, which is larger than the maximum calculated moment of $\sim 4\,\mu_B$/ion based on Hund's rules. Considering the possible fluctuations in Mn concentration characterization, we attributed the situation to a possible isolated ion scheme and the excess per-ion-moment as a consequence of error in Mn concentration estimation. However, in this extended batch of samples, we demonstrated that this anomalously large moment is a robust phenomenon. The previously measured sample is very similar to the Mn 750°C sample in this paper, with similar saturation moment, high
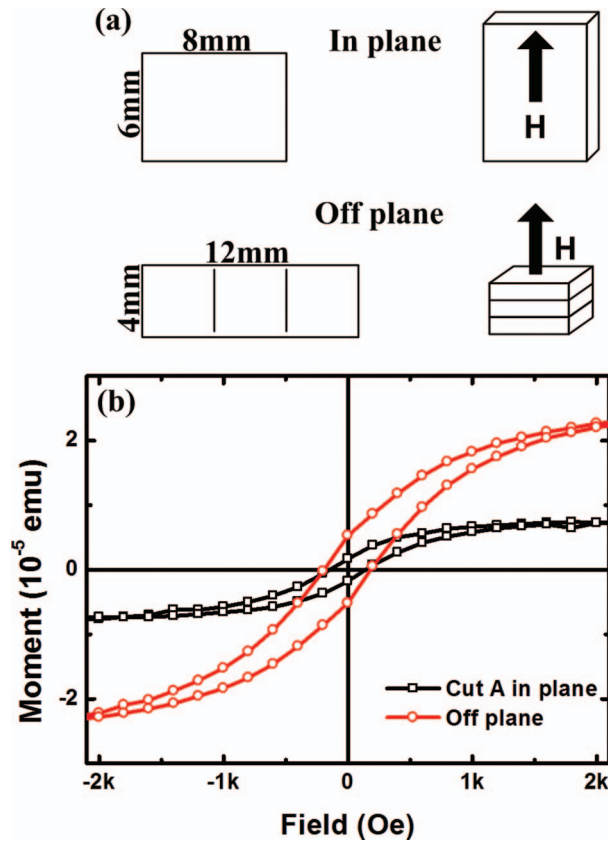
FIG. 9. In-plane/off-plane magnetic anisotropy of Mn doped ZnO sample. (a) Schematic of the samples in this off-plane measurement in comparison to in-plane. The sample was specially cleaved into three small squares and stacked together to provide similar area of thin film, in turn similar amount of Mn doped ZnO to the in-plane sample. (b) M-H hysteresis of Mn cell 800°C sample. Off-plane measurement shows larger saturation moment but similar coercivity field.

coercivity field and high remnant moment. Nevertheless, other samples in this paper exhibit even more peculiar magnetic properties. For example, with a Mn cell temperature of 700°C, using the acquired Mn concentration from SIMS, the saturation moment is quantified to be ∼45 μ_B/ion. What is more, we believe the 'B cut' in our samples is closer to the easy axis of the ferromagnetism than the convenient 'A cut'. When samples in 'B cut' geometry were measured, saturation moments are typically three times larger than that of samples with 'A cut'. This would in turn push the per-ion moment three times larger. XPS and SIMS measurements persistently indicate Mn concentrations smaller than 1%, or 4×10^{20} cm^{-3}. Even if we assume this maximum number of 4×10^{20} cm^{-3} for all samples, the quantified magnetic moment is still very large. In the case of Mn 600°C sample, the saturation moment would amount to ∼13 μ_B/ion for the 'B cut', which is clearly in excess of the expected value for isolated ions.

Finally we discuss a possible mechanism for the large saturated moments in an elimination manner. Contributions from Mn related secondary phases are quite unlikely in our case. The small concentration would minimize phase segregation due to the solubility limit, as confirmed through XRD and XPS measurements. Also, secondary phases would yield smaller magnetic moments than with isolated ions. For the intrinsic mechanisms, firstly given the extremely diluted nature of Mn ions, it is unlikely they can correlate with each other directly to support double exchange[32] or super exchange mechanisms. Also the large per ion moment we observe (at 10-100 μ_B/ion level) does not support such mechanisms, since they cannot provide such large moment.[33] Long distance indirectly coupled ions may be a contributing mechanism, and the measured relatively abundant carrier concentration should permit it. However, the measured moment being larger than single ion moment requires some other entities to contribute magnetic moment as well. This leads to
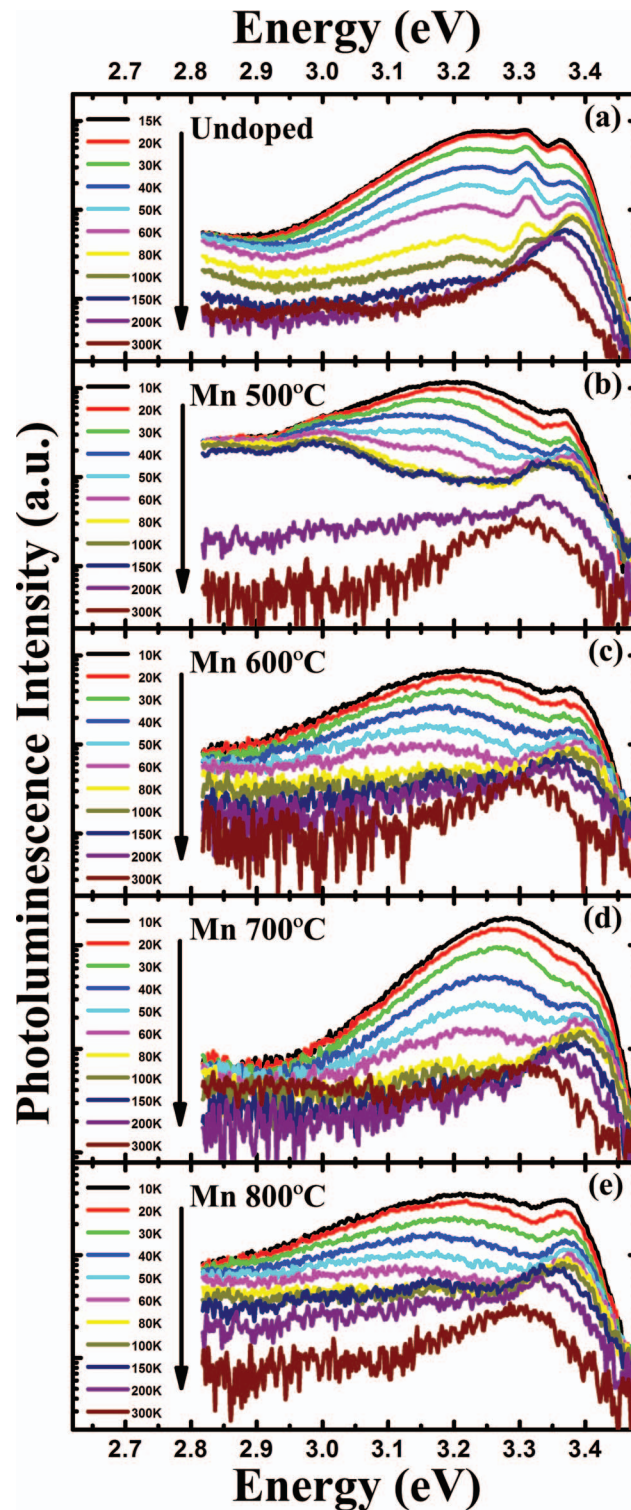
FIG. 10. Temperature dependent PL of (a) undoped ZnO and (b) ~ (e) Mn doped ZnO with Mn cell temperature of 500°C ~ 800°C. Undoped ZnO sample shows donor bound exciton at ~3.362eV, TES peak at ~3.308eV, and its phonon replica at lower energy, indicating good quality. Similar behavior is observed in Mn 700°C sample. The other Mn doped samples only show DX at ~3.36eV, with broad luminescence bump at ~3.2eV range.
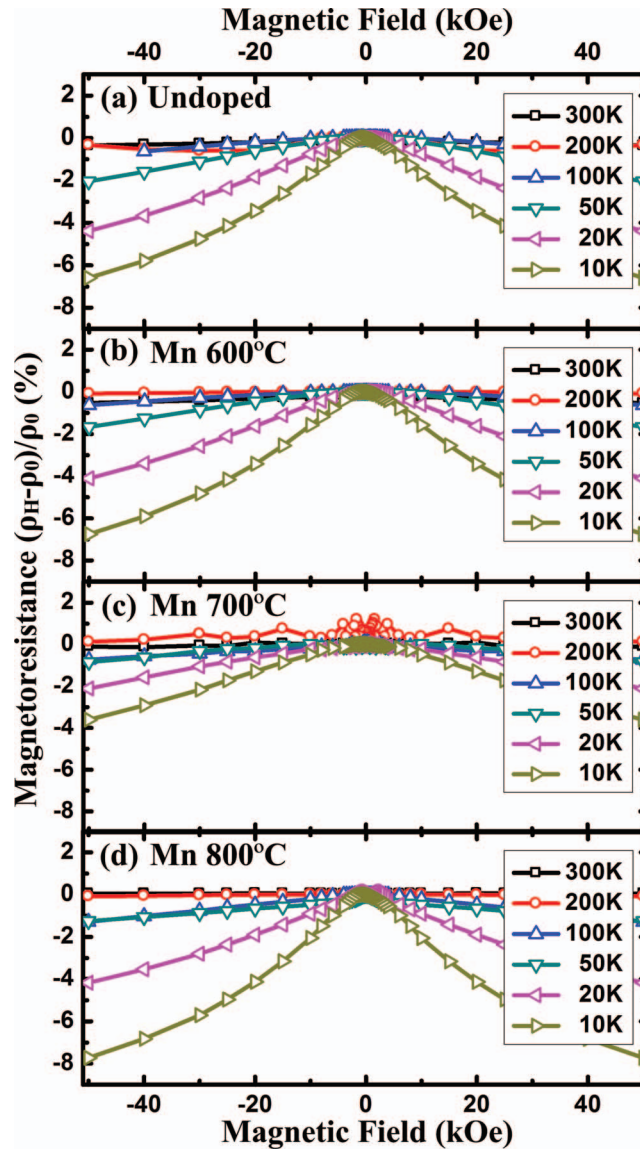
FIG. 11. Magneto resistance (MR) of (a) undoped ZnO and (b) $\sim$ (d) Mn doped ZnO. Undoped ZnO shows typical negative MR, which increases as temperature lowers. Mn doped films have similar MR behavior like that of undoped ZnO, but have more evident trend of positive MR. This is most evident at Mn cell 700C sample, which shows entirely positive MR at 200K.

a situation close to the BMP mechanism, where multiple species can correlate and contribute to ferromagnetism.[21] No evident ferromagnetism for undoped and very low doping samples indicates that Mn dopant still acts as a crucial factor for the RT ferromagnetism. It is possible that point defects or zinc nuclei form the BMP centered on Mn ions. However, one argues that BMP theory would not result in such large moments, i.e. magnetic moments reaching 10-100 μ_B/ion as in our case. We note that types of investigations on materials with such low dopant concentrations are rarely reported. As a result of this research, a new understanding of the mechanisms behind intrinsic ferromagnetism in a DMS system with low transition-metal ion concentrations is necessary.

IV. SUMMARY

We have observed peculiarly strong room temperature ferromagnetism in lightly Mn doped ZnO thin films. Both in-plane and out-of-plane magnetic anisotropy were observed to support intrinsic
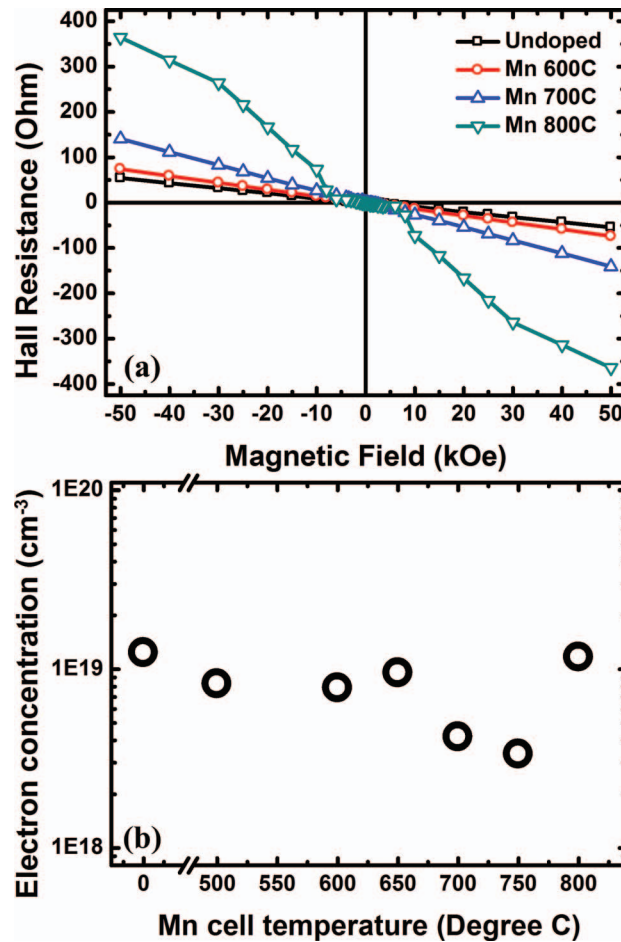
FIG. 12. (a) Hall effect data of undoped and Mn doped ZnO samples at 10K. It is evident that Mn 800°C sample has an exceptionally large anomalous Hall effect, in comparison to other samples. (b) Room temperature carrier concentration data showing only a small variance in the range of $10^{18} \sim 10^{19}$ cm^{-3}.

ferromagnetism. Both the saturation moment and coercivity field vary with different Mn content. The observed magnetic moment when expressed in terms of the number of μB/ion exceeds what calculated for isolated Mn ions. Contributions from other local entities are necessary, but the absence of ferromagnetism in undoped ZnO confirms the crucial role of the Mn dopant. The result supports intrinsic ferromagnetism of Mn doped ZnO, while raises a challenging question on the origin of room temperature ferromagnetism in DMS system with low transition-metal ion concentrations.

ACKNOWLEDGMENTS

[1] T. Dietl, H. Ohno, F. Matsukura, J. Cibert, and D. Ferrand, Science **287**, 1019 (2000).
[2] D. D. Awschalom and M. E. Flatte, Nature Physics **3**, 153 (2007).
[3] S. B. Ogale, Adv. Mater. **22** 3125 (2010).
[4] A. H. Macdonald, P. Schiffer, and N. Samarth, Nature Materials **4**, 195 (2005).
[5] K. Sato and H. Katayama-Yoshida, Jpn. J. Appl.Phys. **40**, L334 (2001).

[6] S. W. Jung, S. J. An, Gyu-Chul Yi, C. U. Jung, Sung-Ik Lee, and Sunglae Cho, Appl. Phys. Lett. **80**, 4561 (2002).

[7] J. Alaria, P. Turek, M. Bernard, M. Bouloudenine, A. Berbadj, N. Brihi, G. Schmerber, S. Colis, and A. Dinia, Chem. Phys. Lett. **415**, 337 (2005).

[8] P. Shama, A. Gupta, K. V. Rao, F. J. Owens, R. Shama, R. Ahuja, J. M. Osorio Guillen, B. Johansson, and G. A. Gehring, Nature Materials **2**, 673 (2003).

[9] Y. F. Tian, Y. F. Li, M. He, I. A. Putra, H. Y. Peng, B. Yao, S. A. Cheong, and T. Wu, Appl. Phys. Lett. **98**, 162503 (2011).

[10] D. P. Norton, M. E. Overberg, S. J. Pearton, K. Pruessner, J. D. Budai, L. A. Boatner, M. F. Chisholm, J. S. Lee, Z. G. Khim, Y. D. Park, and R. G. Wilson, Appl. Phys. Lett. **83**, 5488 (2003).

[11] Z. Yang, J. L. Liu, M. Biasini, and W. P. Beyermann, Appl. Phys. Lett. **92**, 042111 (2008).

[12] Z. Yang, W. P. Beyermann, M. B. Katz, O. K. Ezekoye, Z. Zuo, Y. Pu, J. Shi, X. Q. Pan, and J. L. Liu, J. Appl. Phys. **105**, 053708 (2009).

[13] X. M. Cheng and C. L. Chien, J. Appl. Phys. **93**, 7876 (2003).

[14] T. Fukumura, Z. Jin, M. Kawasaki, T. Shono, T. Hasegawa, S. Koshihara, and H. Koinuma, Appl. Phys. Lett. **78**, 958 (2001).

[15] C. Tuan, J. D. Bryan, A. B. Pakhomov, V. Shutthanandan, S. Thevuthasan, D. E. Mccready, D. Gaspar, M. H. Engelhard, J. W. Rogers, Jr., K. Krishnan, D. R. Gamelin, and S. A. Chambers, Phys. Rev. B **70**, 054424 (2004).

[16] X. J. Wang, I. A. Buyanova, W. M. Chen, C. J. Pan, and C. W. Tu, J. Appl. Phys. **103**, 023712 (2008).

[17] Z. Yang, Z. Zuo, H. Zhou, W. P. Beyermann, and J. Liu, J. Crys. Grow. **314**, 97 (2011).

[18] Z. Zuo, H. Zhou, M. J. Olmedo, J. Kong, W. P. Beyermann, J. G. Zheng, Y. Xin, and J. Liu, J. Appl. Phys. **112**, 125103 (2012).

[19] C. Liu, F. Yun, and H. Morkoc, J. Mater. Sci. Mater. Elec. **16**, 555 (2005).

[20] G. Lawes, A. S. Risbud, A. P. Ramirez, and R. Seshadri, Phys.Rev. B **71**, 045201 (2005).

[21] J. M. D Coey, M. Venkatesan, and C. B. Fitzgerald, Nature Materials **4** 173 (2005).

[22] A. C. Durst, R. N. Bhatt, and P. A. Wolff, Phys. Rev. B **65** 235205 (2002).

[23] Q. Wang, Q. Sun, P. Jena, and Y. Kawazoe, Phys. Rev. B **79**, 115407 (2009).

[24] K. R. Kittilstved, N. S. Norberg, and D. R. Gamelin, Phys. Rev. Lett. **94**, 147209 (2005).

[25] T. Fukumura, Z. Jin, A. Ohtomo, H. Koinuma, and M. Kawasaki, Appl. Phys. Lett. **75**, 3366 (1999).

[26] M. A. Garcia, E. Fernandez Pinel, J. de la Venta, A. Quesada, V. Bouzas, J. F. Fernández, J. J. Romero, M. S. Martín González, and J. L. Costa-Krämer, J. Appl. Phys. **105**, 013925 (2009).

[27] M. R. Wagner, G. Callsen, J. S. Reparaz, J.-H. Schulze, R. Kirste, M. Cobet, I. A. Ostapenko, S. Rodt, C. Nenstiel, M. Kaiser, A. Hoffmann, A. V. Rodina, M. R. Phillips, S. Lautenschläger, S. Eisermann, and B. K. Meyer, Phys. Rev. B **84** 035313 (2011).

[28] Ü. Özgür, Ya. I. Alivov, C. Liu, A. Teke, M. A. Reshchikov, S. Doğan, V. Avrutin, S.-J. Cho, and H. Morkoç, J. Appl. Phys. **98**, 041391 (2005).

[29] A. Teke, Ü. Özgür, S. Doğan, X. Gu, H. Morkoç, B. Nemeth, J. Nause, and H. O. Everitt, Phys. Rev. B **70**, 195207 (2004).

[30] T. Andrearczyk, J. Jaroszyński, G. Grabecki, T. Dietl, T. Fukumura, and M. Kawasaki, Phys. Rev. B **72**, 121309R (2005).

[31] M. Gacic, G. Jakob, C. Herbort, and H. Adrian, Phys. Rev. B **75**, 205206 (2007).

[32] M. A. García, M. L. Ruiz-González, A. Quesada, J. L. Costa-Krämer, J. F. Fernández, S. J. Khatib, A. Wennberg, A. C. Caballero, M. S. Martín-González, M. Villegas, F. Briones, J. M. González-Calbet, and A. Hernando, Phys. Rev. Lett. **94**, 217205 (2005).

[33] T. Dietl, Nature Materials **9**, 965 (2010).